Adsorption and separation of linear and branched alkanes on carbon nanotube bundles from configurational-bias Monte Carlo simulation

Jianwen Jiang,[1,*] Stanley I. Sandler,[1] Merijn Schenk,[2] and Berend Smit[2]
[1]*Department of Chemical Engineering, University of Delaware, Newark, Delaware 19716, USA*
[2]*Department of Chemical Engineering, University of Amsterdam, Nieuwe Achtergracht 166, 1018 WV Amsterdam, The Netherlands*
(Received 20 February 2005; published 27 July 2005)

The adsorption and separation of linear (C_1-nC_5) and branched (C_5 isomers) alkanes on single-walled carbon nanotube bundles at 300 K have been studied using configurational-bias Monte Carlo simulation. For pure linear alkanes, the limiting adsorption properties at zero coverage exhibit a linear relation with the alkane carbon number; the long alkane is more adsorbed at low pressures, but the reverse is found for the short alkane at high pressures. For pure branched alkanes, the linear isomer adsorbs to a greater extent than its branched counterpart. For a five-component mixture of C_1-nC_5 linear alkanes, the long alkane adsorption first increases and then decreases with increasing pressure, but the short alkane adsorption continues increasing and progressively replaces the long alkane at high pressures due to the *size entropy* effect. All the linear alkanes adsorb into the internal annular sites with preferred alignment parallel to the nanotube axis on a bundle with a gap of 3.2 Å, and also intercalate the interstitial channels in a bundle with a gap of 4.2 Å. For a three-component mixture of C_5 isomers, the adsorption of each isomer increases with increasing pressure until saturation, though nC_5 increases more rapidly with pressure and is preferentially adsorbed due to the *configurational entropy* effect. All the C_5 isomers adsorb into the internal annular sites on a bundle with a gap of 3.2 Å, but only nC_5 also intercalates the interstitial channels on a bundle with a gap of 4.2 Å. This work suggests the possibility of separating alkane mixtures based on differences in either size or configuration, as a consequence of competitive adsorption on the carbon nanotube bundles.

DOI: 10.1103/PhysRevB.72.045447 PACS number(s): 68.43.−h, 81.05.Rm, 05.70.−a

I. INTRODUCTION

The adsorption and separation of alkanes in porous media play a significant role in various disciplines of natural science and underlie many engineering processes and industrial applications. For instance, many volatile organic compounds classified as atmospheric pollutants are directly or indirectly related to alkanes and their derivatives, and adsorption is currently one of the technically feasible and cost effective technologies to remove and recover these compounds.[1] The catalytic conversion and cracking of alkanes are major reactions in the petrochemical refinery industry, and the simultaneous alkane adsorption on catalysts or catalyst supports has been found to be important to interpret kinetic data.[2] Many industrial processes involve alkane mixtures, and how to separate them for particular use is an important topic. Usually alkane isomers have close boiling points, e.g., 309.2, 301.1, and 282.6 K at 1 atm for nC_5, iC_5, and $neoC_5$,[3] and it is difficult to separate them using conventional methods such as distillation. But with a proper choice of adsorbents (or molecular sieves) and operating conditions, alkanes may be separated by competitive adsorption based on the differences in their molecular size and shape.[4–6]

Over years, numerous experimental studies have been carried out on the adsorption and separation of alkanes on various types of adsorbents. Maciver *et al.*[7] measured the adsorption of lower molecular weight alkanes (C_3, nC_4 and iC_4) on silica, alumina, and silica-alumina cracking catalysts over the temperature range from 25 ° to 350 °C, and observed physisorption accompanied by chemisorption. Bruce *et al.*[8] determined the gas-solid second virial coefficients for the normal C_3, C_4, C_5, and C_6 alkanes on Carbopack C and C-HT in the temperature range of 323 to 471 K, and found that the gas-solid adsorption energy has a linear correlation with the boiling point and with the ratio of critical temperature to the square root of the critical pressure. Denayer *et al.*[9] determined the Henry constants, limiting adsorption enthalpies, van't Hoff pre-exponential factors, and separation factors of C_5–C_8 alkanes on a variety of zeolites at 473–648 K, and found both nonselective and selective adsorption between linear and branched alkanes dependent on the zeolite type. Denayer *et al.*[10] also found that competitive adsorption, rather than diffusion, is the major factor in controlling the hydrocracking order of the *n*-alkanes on Pt/H-Y zeolite. Savitz *et al.*[11] measured the isosteric heats and adsorption isotherms of the C_1, C_2, and C_3 alkanes on a series of six high-silica zeolites, and observed an inverse relationship between the limiting isosteric heat and the pore diameter. Yun *et al.*[12] reported the adsorption of the C_1 and C_2 alkanes, and their binary mixtures on hexagonally ordered MCM-41, and validated methods for the prediction of adsorption equilibrium. Hernandez *et al.*[13] measured the adsorption capacities of the linear C_6, C_7, C_8, and C_9 alkanes on microporous silica solids at different temperatures, and found the limiting adsorption energy to be more attractive for a longer alkane.

With substantial improvements in computational power over the last few decades, molecular simulation methods, including Monte Carlo (MC) and molecular dynamics (MD), have increasingly become a useful tool to investigate the properties of fluids confined in porous materials.[14] Simulations can provide insights into the microscopic picture of molecules adsorbed in a confined space and enable one to

examine the underling physics, which may be inaccessible to experiments. For the simulation of alkane adsorption in porous media, MC rather than the MD method is most frequently used for two reasons. First, MD is not likely to provide an adsorption isotherm at a given reservoir condition, which is important in adsorption studies. Second, MD motion mimics the natural behavior of the molecules, that is, how the molecules diffuse into pores before adsorption equilibrium is reached; this is a slow process. In contrast, MC in grand-canonical ensemble (GCMC) permits adsorbate molecules to exchange with the reservoir and can easily yield adsorption isotherms. Also, the MC method does not have to follow the natural pathway and allows a trial move at a random position, so that a successful move may correspond to a large jump in phase space. Consequently, a large number of GCMC simulation studies have been performed on alkane adsorption including, to mention but a few, the adsorption of C_1 in zeolite NaA;[15] of C_1 in zeolites MFI, MOR, and BOG;[16] of C_1, C_2, and their binary mixtures on the one-dimensional (1D) molecular sieve $AlPO_4$-5;[17] of C_1 in metal-organic materials.[18] These simulations on the adsorption of short alkanes used conventional techniques to generate molecular configurations, which can be prohibitively expensive for long alkanes.

A recent advance, the configurational-bias Monte Carlo (CBMC) technique,[19–21] makes the simulation of long alkanes possible. The CBMC method significantly improves the efficiency for sampling of chain-molecule conformations by many orders of magnitude, and its combination with NVT MC and GCMC simulations has been widely used for alkane adsorption, especially, for long alkanes. Smit and Siepmann[22] simulated the adsorption of nC_4 to nC_{12} on silicalite, and a linear dependence of the isosteric heat on chain length was found. Maginn *et al.*[23] examined the low-coverage sorption of normal alkanes from nC_4 to nC_{25} on silicalite, and temperature-dependent alkane configurations and locations were found. Maris *et al.*[24] calculated the adsorption isotherms of C_1 to nC_5 in the aluminophosphate $AlPO_4$-5, and observed a surprisingly low density–high density transition resembling capillary condensation. Du *et al.*[25] simulated adsorption isotherms of pure C_1, C_2, C_3, nC_4, and their binary mixtures on silicalite. Good agreement with limited available experimental data was obtained, and competitive adsorption in the C_1-C_2 mixture was observed in which C_2 is preferentially adsorbed at low pressures but this preference reverses at high pressures. Vlugt *et al.*[26] and Schenk *et al.*[27] simulated the adsorption isotherms of linear and branched alkanes and their binary mixtures on silicalite. A configurational entropy driven "squeezing out" effect was found with a linear alkane progressively replacing its branched counterpart at higher coverages, which was attributed to a higher packing efficiency of the linear alkane within the silicalite channels. Calero *et al.*[28,29] and Krishna *et al.*[30–33] investigated the subtle entropy effects in the adsorption of multicomponent mixtures of linear and branched alkanes, and demonstrated the development of separation processes. De Meyer *et al.*[34] and Chempath *et al.*[35] presented simulations of the liquid-phase adsorption of linear alkanes and their mixtures on ZSM-5 and silicalite, and good agreement with experimental results was obtained. Düren and Snurr[36] computed the adsorption of C_1 and nC_4 and their mixtures on isoreticular metal-organic frameworks, and the influence of the organic linker molecule on adsorption and selectivity were analyzed. Fox *et al.*[37,38] simulated the adsorption of pure and mixed linear, branched, and cyclic alkanes on silicalite-1, $AlPO_4$-5, and ITQ-22, and temperature-dependent adsorption hierarchy and selectivity were found. Also, force fields have been reported for alkane adsorption by calibrating simulation results with reliable experimental data. Dubbeldam *et al.*[39] generated a united-atom force field for linear and branched alkanes on MFI and other zeolites. Calero *et al.*[40] constructed a united-atom force field for linear alkanes on sodium-exchanged FAU-type zeolites. Pascual *et al.*[41] developed a transferable force field for the adsorption of linear and branched alkanes on silicalite-1.

As shown by the above review, most experimental and simulation studies of alkane adsorption were carried out on zeolites. In recent years, carbon nanotubes[42] have stimulated considerable interest, including potential use for membrane adsorption and separation due to their well-defined nanoscale structures.[43]

Experimental studies have been reported on the adsorption of simple pure gases, such as N_2,[44–51] O_2,[49] Ar,[52] Kr,[53] Xe,[54,55] CO_2,[56] on various carbon nanotubes, single- or multi-walled, closed or open ended. H_2 adsorption has also been studied on carbon nanotubes toward developing environmentally friendly fuel cell technology.[57–61] Also, MC simulations have been performed, including the adsorption of N_2,[62,63] Xe,[64] H_2,[65–67] on infinite periodic nanotube bundles, and the adsorption of N_2,[63] Ne,[68,69] Ar,[68,70] Kr,[70] Xe,[68,69] CO_2,[71] H_2,[72,73] on finite isolated nanotube bundles. Only recently have there been a few experimental and simulation investigations on the adsorption of simple gas mixtures on carbon nanotubes, the adsorption of H_2-D_2-T_2 isotope mixtures by path integral GCMC simulation,[74,75] of a NO_x-SO_2-CO_2 mixture in the presence of O_2 by thermogravimetric analysis,[76] of a CF_4-Xe mixture by vibrational spectroscopy and MC simulation,[77] and of a N_2-O_2 mixture (representing air) by GCMC simulation.[78] Competitive adsorption was observed in these studies, and it has been suggested that carbon nanotubes could be a superior adsorptive media to separate gas mixtures.

Questions that remain are as follows: how will carbon nanotubes act in the adsorption and separation of complex alkanes? Can high selectivity be achieved at normal conditions? The few studies in this area have been restricted to pure short linear alkanes, for example, experimental measurements on the adsorption of C_1 (Refs. 53 and 79–81) and nC_4,[82] and simulations on the adsorption of C_1 (Refs. 68, 69, 83, and 84) and C_2.[85] On the other hand, it is worthwhile to point out that MD simulations have been employed to investigate the microscopic behavior of nC_5 and iC_5,[86] and of nC_{10} (Ref. 87) in carbon nanotubes. To the best of our knowledge, however, no experimental or simulation work on the adsorption and separation of alkane mixtures on carbon nanotube bundles has been reported. The objective of this work is to fill this gap using the configurational-bias MC simulation and to determine if carbon nanotubes can be good candidates to separate alkanes. Consequently, first we simulate the adsorption behavior for five pure linear alkanes from

TABLE I. Force field parameters for linear and branched alkanes.

Nonbonded LJ (Refs. 90 and 91)	Site	σ(Å)	ε/k_B(K)
	CH_4	3.73	148.0
	CH_3	3.75	98.0
	CH_2	3.95	46.0
	CH	4.68	10.0
	C	6.40	0.5
Bending (Ref. 92)	$k_\theta/k_B=62500$ K/rad^2	$\theta_0=113.0°$	
Torsion (Ref. 93)	CH_x-CH_2-CH_2-CH_y	CH_x-CH_2-CH-CH_y	
	$v_0/k_B=1009.728$ K	$v_0/k_B=373.0512$ K	
	$v_1/k_B=2018.446$ K	$v_1/k_B=919.0441$ K	
	$v_2/k_B=136.341$ K	$v_2/k_B=268.1541$ K	
	$v_3/k_B=-3164.520$ K	$v_3/k_B=-1737.2160$ K	

C_1 to nC_5, and three pure C_5 isomers, then examine the competitive adsorption for a mixture of C_1-nC_5 linear alkanes with varying chain length, and finally we examine the competitive adsorption for a mixture of C_5 isomers with varying chain branching.

II. MODEL AND POTENTIAL

Two descriptions are commonly used to model alkane molecules, the united-atom model and the all-atom model.[88] Both models were found to give comparable adsorption isotherms for alkane adsorption in silicalite, however, the simpler united-atom model resulted in faster computations.[89] Consequently, the united-atom model representing every CH_x group as a single interaction site was used in this work. The C-C bonds were assumed to be rigid and fixed at 1.53 Å. The nonbonded dispersive interaction between sites of different molecules or four sites apart within a molecule was modeled by the Lennard-Jones (LJ) potential[90,91]

$$u_{\mathrm{LJ}}(r) = 4\varepsilon[(\sigma/r)^{12} - (\sigma/r)^6]. \quad (1)$$

For C_3 and longer alkanes, the intramolecular bond bending between three successive sites was modeled using a harmonic potential[92]

$$u_{\mathrm{bending}}(\theta) = 0.5k_\theta(\theta - \theta_0)^2. \quad (2)$$

For C_4 and longer alkanes, the intramolecular dihedral torsion between four successive sites was modeled using a cosine potential[93]

$$u_{\mathrm{torsion}}(\phi) = \sum_{k=0}^{3} v_k(\cos\phi)^k. \quad (3)$$

The force field parameters, which were optimized by others to accurately reproduce experimental vapor-liquid coexistence curves and critical properties of pure linear and branched alkanes, are given in Table I. The cross LJ parameters for the unlike sites were obtained using the Jorgensen

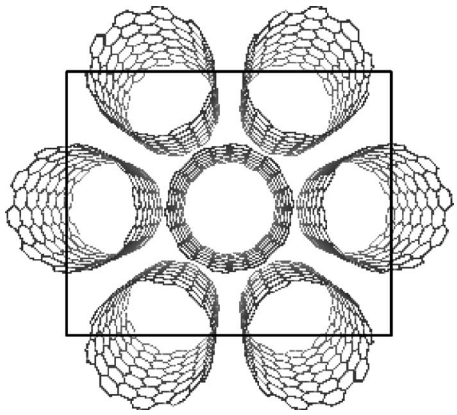

FIG. 1. A periodic hexagonal nanotube bundle. The rectangle illustrates the simulation box in the x and y dimensions.

combining rules $\sigma_{ij}=\sqrt{\sigma_i\sigma_j}$ and $\varepsilon_{ij}=\sqrt{\varepsilon_i\varepsilon_j}$.[94] A spherical cutoff length of 14.5 Å was used for the calculation of the LJ interaction energies, and beyond the cutoff length the usual long-range correction for a homogeneous system was added. The use of the usual long-range correction is an appropriate approximation, because it has been shown that the error introduced by assuming homogeneity is small compared with the magnitude of the long-range correction.[95]

Carbon nanotubes have been experimentally observed to form hexagonal bundles of nearly uniform and finite diameter,[49,96,97] with nanotube numbers between 100 and 500,[96] or of the order of 20.[97] In the simulation study of pure N_2 adsorption on the homogeneous open-ended single-walled carbon nanotube (SWNT) hexagonal bundles at both subcritical and supercritical temperatures,[63] we found that the adsorption isotherm on an infinite periodic bundle without an external surface is of type I regardless of temperature. On a finite isolated bundle with an external surface, the isotherm is of type II at a subcritical temperature and of type I at a supercritical temperature, which is in accord with experimental observations. We also found that the external surface of the nanotube bundle plays an important role on the character for the adsorption isotherm of a N_2-O_2 mixture. However, the N_2-O_2 adsorption selectivity is nearly independent of the nanotube bundle size, though it strongly depends on temperature.[78]

Our objective in this work is to explore the adsorptive separation between alkanes rather than to characterize adsorption isotherm, as a consequence, the infinite periodic bundle as used in our previous studies[63,78] was chosen as the adsorbent model and is illustrated in Fig. 1. A three-dimensional (3D) periodic rectangular parallelepiped of 33.5 Å $\times$ 29.0 Å $\times$ 36.9 Å with hexagonally aligned (10,10) SWNTs was used for the simulation box. There are two kinds of energetically favorable adsorption sites within the bundle, the nanotube interiors and the interstitial channels between the nanotubes. The van der Waals gap g between nanotubes was initially set to 3.2 Å,[33,34] and later in order to examine adsorption in the interstitial channels, $g=4.2$ Å was also used. Each (10, 10) SWNT within the bundle has a diameter of 13.56 Å, and the carbon atoms were assumed to be rigid and frozen during simulation. Recent study of the adsorption

of alkanes in MFI zeolite has revealed that the influence of framework flexibility is quite small,[98] and it is also expected to be so in this work for the low-energy focused equilibrium adsorption.

The dispersive interaction between the carbon atom of nanotube and the united-atom site of alkane was modeled with the LJ potential. The well depth was obtained using the Jorgensen combing rule with $\varepsilon_{C\text{-}C}/k_B=28.0$ K in the nanotube, and the collision diameter was set to 3.6 Å regardless of the type of the united atom. In our previous studies[63,78] the interaction between an adsorbate site and a nanotube was fit to a polynomial function of the radial distance from the nanotube center to accelerate the simulation without a significant loss of accuracy. An alternate accurate and efficient approach was used in the present work. As the adsorbent was assumed to be rigid, its interaction energy with an adsorbate site was tabulated within the adsorbent on a grid space of 0.11 Å before simulation. The interaction energy between the adsorbent and adsorbate at any other position could then be rapidly calculated during simulation by interpolation. A cutoff length of 14.5 Å was also used in the evaluation of the LJ interaction with the usual long-range correction added.

III. SIMULATION METHOD

The conventional MC techniques are prohibitively expensive in sampling the conformation of long alkane molecules, in contrast, the advanced CBMC technique significantly improves the efficiency. Instead of inserting a molecule at a random position, in the CBMC a molecule is grown atom-by-atom biasing energetically favorable configurations while avoiding overlap with other atoms, and the bias is then removed by adjusting the acceptance rules.[99] In this work we have used the CBMC technique in *NVT* MC simulation to calculate limiting properties and in GCMC simulation to calculate isotherms for the adsorption of linear and branched alkanes on the nanotube bundles at temperature $T=300$ K. First, eight trial positions were generated with a probability proportional to $\exp(-\beta U^i_{\text{internal}})$, where $\beta=1/k_BT$ and U^i_{internal} is the internal energy at a position i including the intramolecular bond bending and dihedral torsion interactions. Then one of the trial positions was chosen for growing an atom with a probability proportional to $\exp(-\beta U^i_{\text{external}})/\Sigma_i\exp(-\beta U^i_{\text{external}})$, where U^i_{external} is the external energy including all nonbonded intramolecular and intermolecular Lennard-Jones interactions. In addition, the insertion of molecules was enhanced using the multiple first-bead scheme with 15 trial positions.[100]

Limiting adsorption properties, including the isosteric heat, the Henry constant, the Helmholtz free energy, enthalpy, energy, and entropy for the adsorption of each pure alkane at zero coverage were determined in *NVT* MC simulation using a single alkane molecule. The limiting isosteric heat q^0_{st} was calculated from

$$q^0_{\text{st}} = RT - (\langle U^0_{a,\text{total}}\rangle - \langle U^0_{b,\text{intra}}\rangle), \tag{4}$$

where $\langle U^0_{a,\text{total}}\rangle$ is the ensemble averaged total adsorption energy of the single alkane molecule in the empty bundle, and $\langle U^0_{b,\text{intra}}\rangle$ is that of the single alkane molecule in the bulk phase (the ideal-gas state) due to the intramolecular interactions. These were calculated from

$$\langle U^0_{a,\text{total}}\rangle = N_A \frac{\int u_a(\mathbf{r},\boldsymbol{\varpi})\exp[-\beta u_a(\mathbf{r},\boldsymbol{\varpi})]\mathrm{d}\mathbf{r}\mathrm{d}\boldsymbol{\varpi}}{\int \exp[-\beta u_a(\mathbf{r},\boldsymbol{\varpi})]\mathrm{d}\mathbf{r}\mathrm{d}\boldsymbol{\varpi}}, \tag{5}$$

and

$$\langle U^0_{b,\text{intra}}\rangle = N_A \frac{\int u_{\text{intra}}(\mathbf{r},\boldsymbol{\varpi})\exp[-\beta u_{\text{intra}}(\mathbf{r},\boldsymbol{\varpi})]\mathrm{d}\mathbf{r}\mathrm{d}\boldsymbol{\varpi}}{\int \exp[-\beta u_{\text{intra}}(\mathbf{r},\boldsymbol{\varpi})]\mathrm{d}\mathbf{r}\mathrm{d}\boldsymbol{\varpi}}, \tag{6}$$

where N_A is the Avogadro constant, $\beta=1/k_BT$ and k_B is the Boltzmann constant, $\mathbf{r}$ is the position vector, and $\boldsymbol{\varpi}$ is orientation of the alkane molecule. The Henry constant K_H was calculated from

$$K_H = \frac{N_A}{RT}\frac{\exp(-\beta\mu^0_{\text{ex},a})}{\exp(-\beta\mu^0_{\text{ex},b})} = \frac{N_A}{RT}\frac{\int \exp[-\beta u_a(\mathbf{r},\boldsymbol{\varpi})]\mathrm{d}\mathbf{r}\mathrm{d}\boldsymbol{\varpi}}{\int \exp[-\beta u_{\text{intra}}(\mathbf{r},\boldsymbol{\varpi})]\mathrm{d}\mathbf{r}\mathrm{d}\boldsymbol{\varpi}}, \tag{7}$$

where $\mu^0_{\text{ex},a}$ and $\mu^0_{\text{ex},b}$ are the excess chemical potentials of the single alkane molecule in the empty bundle and of the single alkane molecule itself in bulk phase, respectively. The Helmholtz free energy of adsorption was calculated from

$$\Delta A^0 = \mu^0_a - \mu^0_b = -RT\ln(RTK_H). \tag{8}$$

The adsorption enthalpy was calculated from

$$\Delta H^0 = -q^0_{\text{st}}. \tag{9}$$

The adsorption energy was calculated from

$$\Delta U^0 = RT + \Delta H^0 = \langle U^0_a\rangle - \langle U^0_b\rangle. \tag{10}$$

The adsorption entropy was calculated from

$$\Delta S^0 = (\Delta U^0 - \Delta A^0)/T. \tag{11}$$

In Eqs. (8)–(11), "Δ" refers to the change in a quantity from the bulk phase to the adsorbed phase.

Isotherms for the adsorption of pure alkanes and their mixtures were determined in GCMC simulation with fixed adsorbate chemical potential (fugacity), volume, and temperature. For the conditions of this study, it is acceptable to replace fugacity by pressure, that is, the reservoir is assumed to behave as an ideal gas.[38,41] GCMC simulation has been used widely for the simulation of adsorption as the grand canonical ensemble is an open system in equilibrium with an infinite bulk fluid reservoir, and the number of adsorbate molecules is allowed to fluctuate.

Simulations were carried out for a total of 20 000 cycles, in which the first 10 000 cycles were used for equilibration, and the second 10 000 cycles to obtain ensemble averages. Each cycle consisted of a number of the following attempted trial moves.

(a) *Translation*: A randomly selected molecule is translated with a random displacement in the x, y, or z dimension, and the maximum displacement is adjusted to an overall acceptance ratio of 50%.

(b) *Rotation*: A randomly selected molecule is rotated around the center-of-mass with a random angle, and the maximum angle is adjusted to an overall acceptance ratio of 50%.

(c) *Partial regrowth*: Part of a randomly selected molecule is regrown locally. It is decided at random which part of the molecule is regrown and from which bead the regrowth is started.

(d) *Complete regrowth*: A randomly selected molecule is regrown completely at a random position. From this move in *NVT* MC simulation, which is equivalent to the Widom test-particle insertion method,[101] the excess chemical potential is evaluated.

(e) *Exchange with the reservoir (only in GCMC simulation)*: A molecule is created at a random position, or a randomly selected molecule is deleted. To ensure microscopic reversibility, creation and deletion are attempted at random with equal probability.

(f) *Exchange of molecular identity (only for a mixture in GCMC simulation)*: A molecule is selected randomly and an attempt is made to change its molecular identity. While this trial move is not required in GCMC simulation, its use allows reaching equilibrium faster and reduces fluctuations after equilibration.[102]

The acceptance rules for these trial moves can be found elsewhere.[99] For the adsorption of a pure alkane in *NVT* MC simulation, each cycle consisted of 2000 trial moves (a)–(d), and the relative probabilities for these attempted moves were 10% translation, 10% rotation, 10% partial regrowth, and 70% complete regrowth. For the adsorption of a pure alkane in GCMC simulation, each cycle consisted of 2000 trial moves (a)–(e) with relative probabilities 10% translation, 10% rotation, 10% partial regrowth, 10% complete regrowth, 60% exchange with the reservoir. For the adsorption of a mixture of alkanes in GCMC simulation, the number of trial moves (a)–(f) in each cycle was increased to 5000 to assure mechanical and compositional equilibrium; the relative probability for exchange with the reservoir was decreased to 55%, and a 5% probability was used for the exchange of molecular identity.

TABLE II. Limiting isosteric heats, Henry constants, and adsorption entropies of the pure alkanes adsorption on a bundle with $g=3.2$ Å.

Alkane	q_{st}^0 (kJ/mol)	K_H (mol/dm^3/kPa)	ΔS^0 (J/mol/K)
C_1	18.27	0.03	−18.63
C_2	27.71	0.64	−23.47
C_3	35.86	9.59	−28.24
nC_4	44.66	160.37	−34.36
nC_5	53.36	2646.78	−40.25
$isoC_5$	51.87	1583.59	−39.51
$neoC_5$	47.20	693.85	−30.71

IV. RESULTS AND DISCUSSION

A. Pure linear and branched alkanes

Table II lists the numerical values of the limiting adsorption properties, including isosteric heats q_{st}^0, Henry constants K_H, and adsorption entropies ΔS^0, for the adsorption of the pure linear and branched alkanes on a bundle with $g=3.2$ Å. Although not listed, the values of adsorption enthalpies ΔH^0, energies ΔU^0, and Helmholtz free energies ΔA^0 can be simply calculated using Eqs. (8)–(10). Figure 2 shows (a) isosteric heats, (b) Henry constants, and (c) adsorption entropies, respectively, as a function of N_c, the carbon number of the alkanes. For linear alkanes with differences in size or length, the larger the size (or the longer the length), the greater are the values of the limiting properties. This is expected as the number of the interaction sites in a linear alkane increases with increasing size, and therefore the interaction strength with the nanotube bundle increases. To a good approximation, linear relationships between the limiting properties and N_c are obtained,

$$q_{st}^0 = 8.714 N_c + 9.829, \tag{12}$$

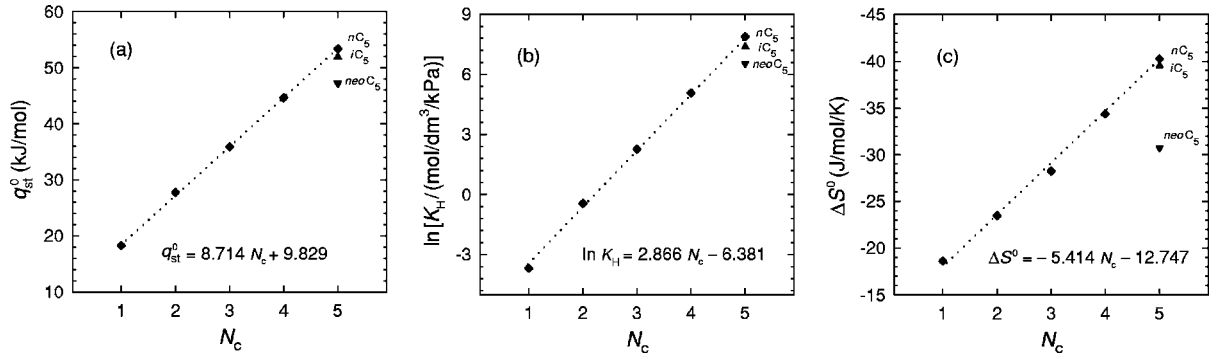

FIG. 2. Limiting adsorption properties of the pure alkanes (C_1, C_2, C_3, nC_4, nC_5, iC_5, and $neoC_5$) on a bundle with $g=3.2$ Å. (a) Isosteric heats, (b) Henry constants, (c) adsorption entropies. Dotted lines are drawn to guide the eye.

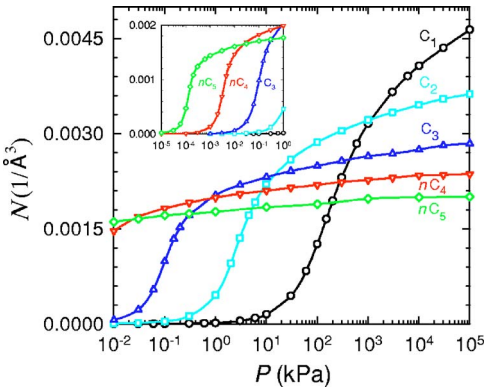

FIG. 3. (Color online) Adsorption isotherms of the pure linear alkanes (C_1,C_2,C_3,nC_4, and nC_5) on a bundle with $g=3.2$ Å.

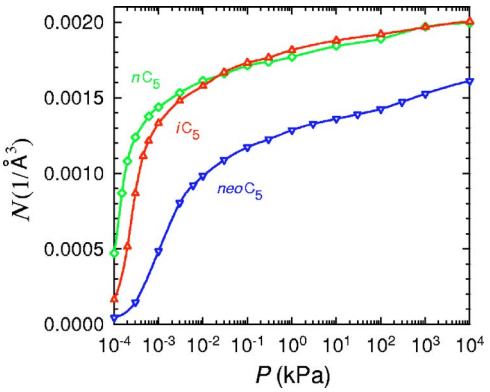

FIG. 4. (Color online) Adsorption isotherms of the pure C_5 isomers (nC_5,iC_5, and $neoC_5$) on a bundle with $g=3.2$ Å.

$$\ln K_H = 2.866N_c - 6.381, \tag{13}$$

$$\Delta S^0 = -5.414N_c - 12.747. \tag{14}$$

Through Eqs. (8)–(10), linear relations can also be derived for ΔH^0,ΔU^0, and ΔA^0. Such linear relations were previously found in the q_{st}^0 for the adsorption of linear alkanes on Carbopack C and C-HT,[8] in the q_{st}^0 and K_H for the adsorption of linear alkanes on silicalite,[22,26,29,31,39,40] and in the q_{st}^0 for the adsorption of linear and branched alkanes on silicalite.[9,41] From these relations, we can estimate the limiting adsorption properties of longer linear alkanes.

For the C_5 isomers with differences in configuration, the greater the degree of branching, the smaller are the values of the limiting adsorption properties. This is a consequence of the decreased packing efficiency within the bundle as the degree of branching increases. Interestingly, compared to nC_5 and iC_5,$neoC_5$ has a much lower absolute value of ΔS^0, indeed even lower than ΔS^0 of nC_4. Again, this is related to alkane configurations in that $neoC_5$ is a pseudospherical molecule, unlike linear alkanes. Upon adsorption and confinement in the nanotube, the configuration of $neoC_5$ is not much changed from that in a bulk fluid, and therefore the entropy loss upon confinement is less than that of the other C_5.

Figure 3 shows the adsorption isotherms of the pure linear alkanes (C_1,C_2,C_3,nC_4, and nC_5 on a bundle with $g=3.2$ Å, expressed as the number of admolecules per unit volume Å^3. At low pressures from 10^{-5} to 10^{-2} kPa shown in the inset, there is considerable adsorption for a long alkane, and almost no adsorption for a short alkane. The number of admolecules decreases with decreasing alkane size because the long alkane has more interaction sites than the short alkane, so energetically the long alkane interacts with the bundle more strongly. At high pressures from 10^3 to 10^5 kPa, however, short alkane is more adsorbed, and the number of admolecules and the saturation coverage increases with decreasing alkane size. This is due to the dominant *size entropy* effect at high coverages, in which small molecules can fit into partially filled pores more easily, and a given volume can hold more small molecules than large molecules. In addition, the long alkane is found to approach saturation at a lower pressure than a short alkane; at 10^3 kPa, the adsorption of nC_5,nC_4, and C_3 is nearly saturated, but not of C_2 and C_1. This observation here is similar to the adsorption of that for pure linear alkanes on silicalite.[26,27,29,31] Over the pressure range in this study, the isotherm of each alkane has only one step to saturation as alkane molecules adsorb almost exclusively into the internal annular sites, although adsorption at the nanotube center is observed for short alkanes at still higher pressures. Accordingly, only one maximum is expected to exist in the isosteric heat of adsorption as a function of coverage, though it was not calculated here. This is different from our previous studies of the adsorption of pure N_2 and a N_2-O_2 mixture on the same nanotube bundle.[63,78] Due to their smaller size, N_2 and O_2 can occupy two types of adsorption sites in a sequential manner, first the internal annular site and then at the nanotube centers, and therefore two steps in the isotherm and two maxima in the isosteric heat were observed.

Figure 4 shows the adsorption isotherms of the pure C_5 isomers (nC_5,iC_5 and $neoC_5$) on a bundle with $g=3.2$ Å. The adsorption of nC_5 is greater than that of iC_5 at low pressures, but they are close at intermediate and high pressures. Compared to nC_5 and iC_5,$neoC_5$ is the least adsorbed over the pressure range under study. The less preferred adsorption of the branched isomer at high coverages has also been seen in the adsorption of the pure C_6 isomers on silicalite.[29,31,32] and is generally attributed to the *configuration entropy* effect, as a result of the bulkier isomer being unable to pack favorably in a confined space due to steric hindrance.

B. A mixture of C_1-nC_5 linear alkanes

Figure 5 shows the adsorption of a five-component mixture of C_1-nC_5 linear alkanes on a bundle with $g=3.2$ Å. The bulk partial pressure ratio of C_1:C_2:C_3:nC_4:nC_5 is 5: 4: 3: 2: 1. The isotherms in Fig. 5(a) show competitive adsorption between the long and short alkanes. With increasing pressure, the long alkane is first adsorbed, passes through a maximum, and then decreases; while the short alkane adsorption continues increasing and progressively replaces the long alkane at high pressures. It is expected that at pressures above those considered here, maximum adsorption will also occur

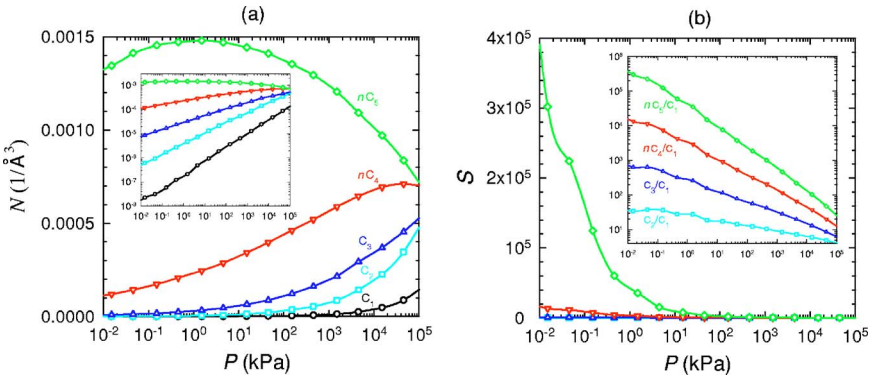

FIG. 5. (Color online) Adsorption of a mixture of linear alkanes (C_1:C_2:C_3:nC_4:nC_5=5:4:3:2:1) on a bundle with g=3.2 Å. (a) Isotherms, (b) selectivities with respect to C_1.

for the short alkane, and finally saturation for all components will be achieved. The pressure at which the maximum adsorption occurs for the long alkane (e.g., nC_5) is lower than for the shorter alkane (e.g., nC_4). At low pressures, the long alkane is preferentially adsorbed as a result of the energetic contribution. The replacement of the long alkane by the short one at elevated pressures is due to the *size entropy* effect, as the small molecule can fit into the partially filled space more easily. This kind of effect has been observed previously, for example, in the simulation studies of the adsorption of linear alkane mixtures on zeolites,[25,29,31,32] of a CF_4-Xe mixture on a nanotube bundle,[77] of N_2-O_2 mixtures on a carbon nanotube bundle,[78] and on C_{168} schwarzite;[103] in the theoretical predictions of the adsorption of hard rods on a linear substrate,[104] of square-well mixtures in one dimension;[105] and also in the experimental measurement of the adsorption of N_2-O_2 mixtures on anatase.[106] Figure 5(b) shows the decreasing adsorption selectivities with increasing pressure of nC_5,nC_4,C_3, and C_2 with respect to the shortest alkane, C_1. Not surprisingly, the greater the difference between two components, the higher is the selectivity. Large values of the selectivity between the long and the short alkanes are obtained at low pressures.

Figure 6(a) shows the radial density distributions $\rho(r)$ of the molecular centers of mass at four pressures (0.015, 1.5, 150, and 15 000 kPa) for the adsorption of the five-component mixture of C_1-nC_5 linear alkanes on a bundle with g=3.2 Å. The $\rho(r)$ is defined as the average number of molecules in an infinitesimal cylindrical bin parallel to the nanotube axis

$$\rho(r) = \langle N(r - \delta r/2, r + \delta r/2)\rangle/(2\pi\, r\, \delta r\, Z), \qquad (15)$$

where r is the radial distance from the center of the bundle, and Z is the nanotube length. At the four pressures, all linear alkanes are observed to adsorb into the internal annular sites, indicated by the peaks in $\rho(r)$ at about 3 Å and by the equilibrium snapshots shown in the insets (carbon nanotubes not shown). A closer look at the density distributions and snapshots reveals the competitive adsorption between long and short alkanes as was also shown in Fig. 5. With increasing pressure from 0.015 to 150 kPa, the peaks of all components increase. However, when pressure is further increased from 150 to 15 000 kPa, the peak of nC_5 decreases; while, the peaks of the other alkanes continue to increase.

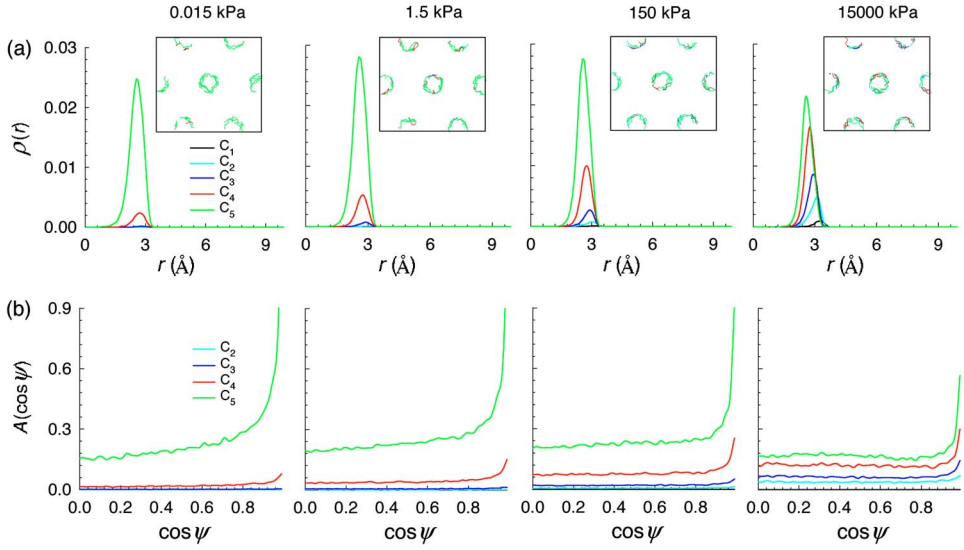

FIG. 6. (Color online) Adsorption of a mixture of linear alkanes (C_1:C_2:C_3:nC_4:nC_5=5:4:3:2:1) on a bundle with g=3.2 Å. (a) Radial density distributions, (b) angular distributions with respect to the z axis.

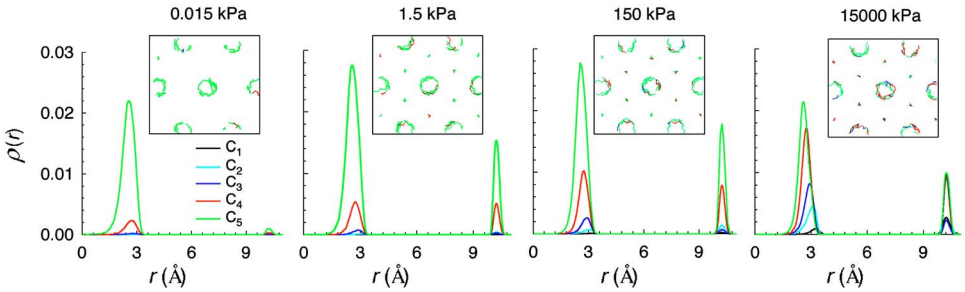

FIG. 7. (Color online) Radial density distributions for the adsorption of a mixture of linear alkanes (C_1:C_2:C_3:nC_4:nC_5 =5:4:3:2:1) on a bundle with g =4.2 Å.

Figure 6(b) shows the angular distributions $A(\cos\psi)$ of the alkane molecules inside a nanotube, where ψ is the angle between the nanotube axis and the end-to-end vector of a linear alkane molecule (except C_1). The range of ψ is from 0° to 180°, however, only one-half of the range from 0° to 90° is shown due to symmetry. The value of $\cos\psi=1$ denotes a molecule parallel to the nanotube axis, and $\cos\psi=0$ denotes perpendicular alignment. The factor $A(\cos\psi)$ is defined as the average number of molecules in an infinitesimal range fo $\cos\psi$,

$$A(\cos\psi) = \langle N(\cos\psi - \delta\cos\psi/2, \cos\psi + \delta\cos\psi/2)\rangle. \tag{16}$$

At a low pressure (0.015 kPa), at which essentially only the long alkane is adsorbed due to strong attraction with adsorbent, $A(\cos\psi)$ has a maximum at $\cos\psi=1$ ($\psi=0°$) and a minimum at $\cos\psi=0$ ($\psi=90°$), and monotonically decreases from $\psi=0°$ to 90 ° . The preferred alignment of the alkane molecules is parallel to the nanotube axis, which favors the packing pattern of the linear alkane inside the 1D nanotube. With increasing pressure, the short alkane replaces the long alkane due to the *size entropy* effect. At a high pressure (15 000 kPa), while the number of nC_5 decreases and numbers of other components increase from those in low pressures (0.0015, 1.5, and 150 kPa), $A(\cos\psi)$ is nearly level from $\cos\psi=0$ to $\cos\psi=1$, except a small maximum at $\psi=0°$. This suggests that the preference for parallel alignment of the alkane molecules is reduced as pressure increases, so that the angular distribution is almost uniform between 0° and 90 °.

To examine adsorption in the interstitial channels between neighboring nanotubes, we also simulated the adsorption of the five-component mixture of C_1-nC_5 linear alkanes on a nanotube bundle with a nanotube gap g=4.2 Å. Adsorption isotherms and selectivities similar to those in Fig. 5 were obtained. Figure 7 shows the radial density distributions $\rho(r)$ of the alkane centers of mass. In this case, in addition to the internal annular sites seen in Fig. 6, the alkane molecules also intercalate the interstitial channels as indicated by peaks at about 10 Å and in the equilibrium snapshots shown in the insets. Because of the narrow attractive region, the linear alkane molecules in the interstitial channels align end-to-end nearly completely parallel to the nanotube axis. The competitive adsorption between the long and short alkanes in this case occurs not only at the internal annular sites as shown in Fig. 6(a), but also in the interstitial channels. The peaks in the radial density distributions of all components at both sites increase with increasing pressure from 0.015 to 150 kPa. However, as the pressure is increased from 150 to 15 000 kPa, the peaks of nC_5 at both sites are reduced, while the peaks of all the other alkanes at both sites continue increasing.

A mixture of C_5 isomers

Figure 8 shows the adsorption of a three-component mixture of C_5 isomers on a bundle with g=3.2 Å at the bulk partial pressure ratio of nC_5:iC_5:$neoC_5$=1: 1: 1. Figure 8(a) shows the isotherms evidencing competitive adsorption between the linear and branched isomers. With increasing pressure, the adsorption of each isomer increases, but the adsorption of nC_5 increases more rapidly with pressure at low pressures and has a higher saturation value at high pressures. The nC_5 is preferentially adsorbed over the branched isomers due to the *configurational entropy* effect as the packing efficiency within the nanotube is greater with a lower degree of branching. This is in accord with the concept of shape selectivity, that is, a slender alkane is preferentially adsorbed over

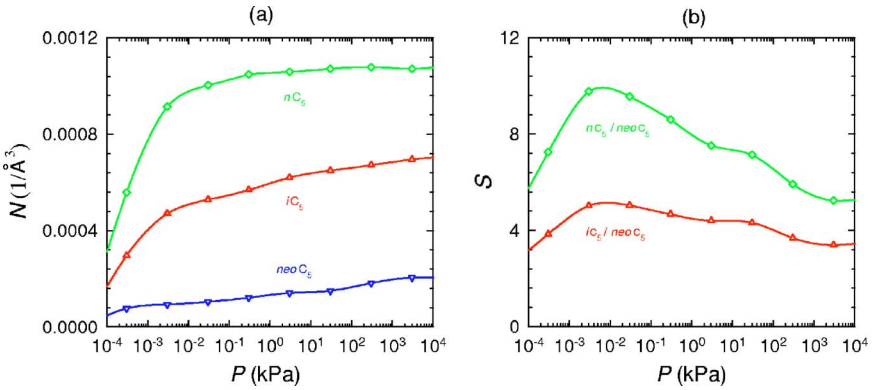

FIG. 8. (Color online) Adsorption of a mixture of C_5 isomers (nC_5:iC_5:$neoC_5$=1:1:1) on a bundle with g=3.2 Å. (a) Isotherms, (b) selectivities with respect to $neoC_5$.

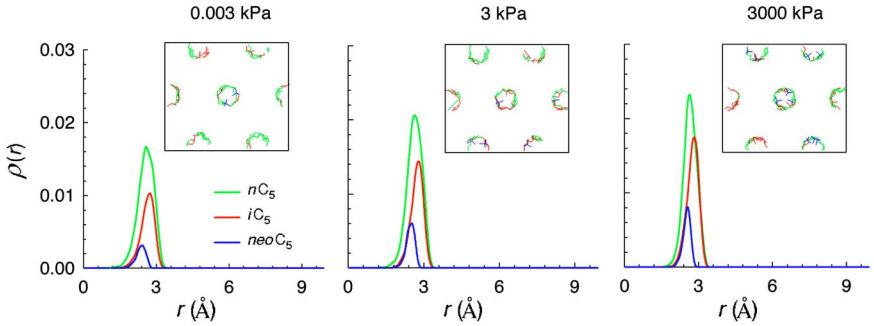

FIG. 9. (Color online) Radial density distributions for the adsorption of a mixture of C_5 isomers (nC_5:iC_5:$neoC_5$=1:1:1) on a bundle with g=3.2 Å.

a bulky one. This has been observed in the adsorption of mixtures of linear and branched alkanes on MFI zeolite.[26,27,29,31,32] Figure 8(b) shows the selectivities of nC_5 and iC_5 relative to $neoC_5$. With increasing pressure, the selectivity first increases and then decreases to a constant value near saturation. Though the values of selectivity here are not as large as in Fig. 5(b), adsorptive separation between the C_5 isomers is still possible.

Figure 9 shows the radial density distributions $\rho(r)$ of the molecular centers of mass at three pressures (0.003, 3, and 3000 kPa) for the adsorption of the mixture of C_5 isomers on a bundle with g=3.2 Å. At the three pressures, as in Fig. 6(a), all alkane molecules adsorb into only the internal annular sites as shown by the peaks at about 3 Å and the equilibrium snapshots in the insets. The peaks of all components increase with increasing pressure from 0.003 to 3000 kPa.

To examine adsorption in the interstitial channels, the adsorption of the three-component mixture of C_5 isomers on a bundle with g=4.2 Å was also studied. The adsorption isotherms and selectivities are very similar to those in Fig. 8 and therefore are not shown here. Figure 10 shows the radial density distributions $\rho(r)$ of the molecular centers of mass. In this case, although all isomers adsorb into the internal annular sites, only nC_5 but not iC_5 or $neoC_5$ can intercalate the interstitial channels. With increasing pressure from 0.003 to 3000 kPa, the peaks of all three isomers at the internal annular sites and the peak of nC_5 in the interstitial channels increase. The behavior here is different from the adsorption of the mixture of C_1-nC_5 linear alkanes on a bundle with g =4.2 Å shown in Fig. 7, in which all the linear alkanes can intercalate the interstitial channels. This is because the interstitial channel has a narrow attractive region, and only the linear alkane molecules when parallel to the nanotube axis can enter. This adsorption phenomenon suggests that with a careful choice of the gap in carbon nanotube bundles, the interstitial channels might act as molecular sieves to efficiently separate linear and branched alkanes.

V. CONCLUSIONS

We have investigated the adsorption of pure linear and branched alkanes and their mixtures on (10, 10) single-walled carbon nanotube bundles using configurational-bias Monte Carlo simulations. The limiting adsorption properties for pure linear alkanes are found to be linearly related to their carbon number, which permits one to estimate the limiting properties for longer linear alkanes. Competitive adsorption occurs in alkane mixtures as a consequence of size and/or configurational differences between the components. For a mixture of linear alkanes, the energetic contribution prevails at low pressures and the long alkane is preferentially adsorbed; however, the size entropy effect becomes more important at high pressures and the short alkane progressively replaces the long alkane. For a mixture of linear and branched isomers, the configurational entropy effect dominates, and there is greater adsorption of the linear isomer. The selectivities of the different alkanes simulated imply that it may be possible to produce adsorptive separation between alkane mixtures using carbon nanotubes. All the alkane molecules adsorb only into the internal annular sites with a preferential packing parallel to the nanotube axis on a bundle with gap of 3.2Å. However, only the linear alkane molecules intercalate the interstitial channels and they are nearly completely parallel to the nanotube axis on a bundle with gap of 4.2Å.

It is worth noting that the nonbonded interaction potential between the alkane and the carbon nanotube was estimated empirically in this work. Such a potential may not be accurate because the interaction might be influenced by the nanotube curvature, which could change the localization of the

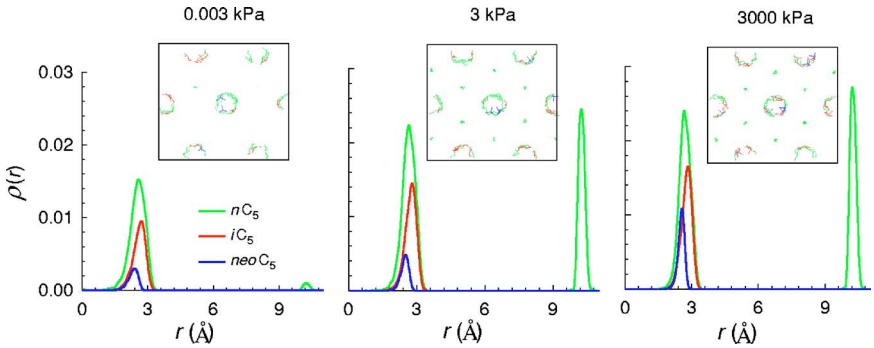

FIG. 10. (Color online) Radial density distributions for the adsorption of a mixture of C_5 isomers (nC_5:iC_5:$neoC_5$=1:1:1) on a bundle with g=4.2 Å.

electron density. In fact, the curvature-induced charge redistribution and polarization in curved carbon nanotubes have been recognized,[107] and the force field parameters of the gas-carbon interaction potential in carbon nanotubes have been found to be curvature dependent.[108] To account for the influence of surface curvature, an accurate interaction potential obtained, for example, from quantum chemical calculations should be used. However, the interaction governing adsorption behavior here is mainly dispersive van der Waals forces, which are difficult to calculate accurately from quantum chemistry unless with sufficiently high level theory, very large basis set, and a great deal of CPU time is used. Alternatives are to use hybrid techniques, as proposed by Clark *et al.*,[109] in which the dispersive interactions are incorporated by *ad hoc* empirical potentials; or using the HM-IE method[110] as we have used to calculate the *ab initio* potentials of O_2 and N_2 with C_{168} schwarzite and C_{60}, respectively.[111–113] While we expect the use of a more accurate potential might lead to some quantitative differences from the results using the empirical potential, we do not expect any qualitative differences.

ACKNOWLEDGMENTS

Two of the authors (J.J. and S.I.S.) gratefully acknowledge the financial support from Grant No. DE-FG02-85ER13436 of the U.S. Department of Energy, and Grant No. CTS-0083709 of the U.S. National Science Foundation. One of the authors (B.S.) acknowledges the support of The Netherlands Research Council for Chemical Sciences (CW) through PIONIER.

*Corresponding author. Tel: 302-831-6953; Fax: 302-831-1048; E-mail address: jiangj@che.udel.edu

[1] M. Lordgooei, M. J. Rood, and M. R. Abadi, Environ. Sci. Technol. **35**, 613 (2001).
[2] W. O. Haag, in *Zeolites and Related Microporous Materials: State of the Art 1994, Studies in Surface Science and Catalysis*, edited by J. Weitkamp, H. G. Karge and H. Pfeifer (Elsevier, Amsterdam, 1994), Vol. 84, p. 1375.
[3] P. J. Linstrom and W. G. Mallard, *NIST Chemistry Webbook* (National Institute of Standards and Technology, Gaithersburg MD, 2003).
[4] S. M. Csicsery, Pure Appl. Chem. **58**, 841 (1986).
[5] N. Y. Chen, W. E. Garwood, and F. G. Dwyer, *Shape Selective Catalysis in Industrial Applications* (Dekker, New York, 1989).
[6] J. M. Thomas, Sci. Am. **266**, 82 (1992).
[7] D. S. Maciver, P. H. Emmett, and H. S. Frank, J. Phys. Chem. **62**, 935 (1958).
[8] C. D. Bruce *et al.*, J. Colloid Interface Sci. **194**, 448 (1997).
[9] J. F. Denayer *et al.*, J. Phys. Chem. B **102**, 4588 (1998).
[10] J. F. Denayer, *et al.*, Ind. Eng. Chem. Res. **36**, 3242 (1997).
[11] S. Savitz, *et al.*, J. Phys. Chem. B **102**, 6865 (1998).
[12] J. H. Yun, *et al.*, Langmuir **18**, 2693 (2002).
[13] M. A. Hernandez *et al.*, Energy Fuels **17**, 262 (2003).
[14] C. R. A. Catlow, R. A. van Santen, and B. Smit, *Computer Modelling of Microporous Materials* (Elsevier, Amsterdam, 2004).
[15] P. R. Van Tassel, H. T. Davis, and A. V. McCormick, Langmuir **10**, 1257 (1994).
[16] L. A. Clark, A. Gupta, and R. Q. Snurr, J. Phys. Chem. B **102**, 6720 (1998).
[17] P. Adhangale and D. Keffer, Langmuir **18**, 10455 (2002).
[18] T. Duren, *et al.*, Langmuir **20**, 2683 (2004).
[19] J. I. Siepmann and D. Frenkel, Mol. Phys. **75**, 59 (1992).
[20] D. Frenkel, G. C. A. M. Mooij, and B. Smit, J. Phys.: Condens. Matter **4**, 3053 (1992).
[21] J. J. de Pablo, M. Laso, and U. W. Suter, J. Chem. Phys. **96**, 2395 (1992).
[22] B. Smit and J. I. Siepmann, Science **264**, 1118 (1994).
[23] E. J. Maginn, A. T. Bell, and D. N. Theodorou, J. Phys. Chem. **99**, 2057 (1995).
[24] T. Maris, T. J. H. Vlugt, and B. Smit, J. Phys. Chem. B **102**, 7183 (1998).
[25] Z. M. Du, *et al.*, AIChE J. **44**, 1756 (1998).
[26] T. J. H. Vlugt, R. Krishna, and B. Smit, J. Phys. Chem. B **103**, 1102 (1999).
[27] M. Schenk, *et al.*, Langmuir **17**, 1558 (2001).
[28] S. Calero, B. Smit, and R. Krishna, J. Catal. **202**, 395 (2001).
[29] S. Calero, B. Smit, and R. Krishna, Phys. Chem. Chem. Phys. **3**, 4390 (2001).
[30] R. Krishna and B. Smit, Chem. Innovation **31**, 27 (2001).
[31] R. Krishna, S. Calero, and B. Smit, Chem. Eng. J. **88**, 81 (2002).
[32] R. Krishna, B. Smit, and S. Calero, Chem. Soc. Rev. **31**, 185 (2002).
[33] B. Smit and R. Krishna, Chem. Eng. Sci. **58**, 557 (2003).
[34] K. M. A. De Meyer, *et al.*, J. Phys. Chem. B **107**, 10760 (2003).
[35] S. Chempath, *et al.*, Langmuir **20**, 150 (2004).
[36] T. Duren and R. Q. Snurr, J. Phys. Chem. B **108**, 15703 (2004).
[37] J. P. Fox, V. Rooy, and S. P. Bates, Microporous Mesoporous Mater. **69**, 9 (2004).
[38] J. P. Fox and S. P. Bates, J. Phys. Chem. B **108**, 17136 (2004).
[39] D. Dubbeldam *et al.*, J. Phys. Chem. B **108**, 12301 (2004).
[40] S. Calero *et al.*, J. Am. Chem. Soc. **126**, 11377 (2004).
[41] P. Pascual *et al.*, Phys. Chem. Chem. Phys. **5**, 3684 (2003).
[42] S. Iijima, Nature (London) **354**, 56 (1991).
[43] P. M. Ajayan and O. Z. Zhou, *Carbon Nanotubes* (Springer-Verlag, Berlin, 2001), Vol. 80, p. 391.
[44] D. Ciuparu *et al.*, J. Phys. Chem. B **108**, 503 (2004).
[45] J. I. Paredes *et al.*, J. Phys. Chem. B **107**, 8905 (2003).
[46] D. H. Yoo *et al.*, J. Phys. Chem. B **107**, 1540 (2003).
[47] D. H. Yoo *et al.*, J. Phys. Chem. B **106**, 3371 (2002).
[48] K. Murata *et al.*, J. Phys. Chem. B **105**, 10210 (2001).
[49] A. Fujiwara *et al.*, Chem. Phys. Lett. **336**, 205 (2001).
[50] E. Alain *et al.*, *Characterization of Porous Solids V* (Elsevier Science, Amsterdam, 2000), Vol. 128, p. 313.
[51] S. Inoue *et al.*, J. Phys. Chem. B **102**, 4689 (1998).
[52] D. H. Yoo *et al.*, J. Phys. Chem. B **106**, 9000 (2002).
[53] M. Muris *et al.*, Langmuir **16**, 7019 (2000).
[54] A. Kuznetsova *et al.*, J. Chem. Phys. **115**, 6691 (2001).
[55] A. Kuznetsova *et al.*, J. Chem. Phys. **112**, 9590 (2000).

[56] M. Cinke *et al.*, Chem. Phys. Lett. **376**, 761 (2003).
[57] A. Zuttel *et al.*, Int. J. Hydrogen Energy **27**, 203 (2002).
[58] F. L. Darkrim, P. Malbrunot, and G. P. Tartaglia, Int. J. Hydrogen Energy **27**, 193 (2002).
[59] H. M. Cheng, Q. H. Yang, and C. Liu, Carbon **39**, 1447 (2001).
[60] R. G. Ding *et al.*, J. Nanosci. Nanotechnol. **1**, 7 (2001).
[61] A. C. Dillon and M. J. Heben, Appl. Phys. A: Mater. Sci. Process. **72**, 133 (2001).
[62] Y. F. Yin, T. Mays, and B. McEnaney, Langmuir **15**, 8714 (1999).
[63] J. W. Jiang and S. I. Sandler, Phys. Rev. B **68**, 245412 (2003).
[64] V. V. Simonyan *et al.*, J. Chem. Phys. **114**, 4180 (2001).
[65] D. Levesque *et al.*, J. Phys.: Condens. Matter **14**, 9285 (2002).
[66] C. Gu *et al.*, Int. J. Hydrogen Energy **26**, 691 (2001).
[67] V. V. Simonyan, P. Diep, and J. K. Johnson, J. Chem. Phys. **111**, 9778 (1999).
[68] M. M. Calbi and M. W. Cole, Phys. Rev. B **66**, 115413 (2002).
[69] M. M. Calbi *et al.*, J. Chem. Phys. **115**, 9975 (2001).
[70] S. M. Gatica *et al.*, J. Chem. Phys. **114**, 3765 (2001).
[71] C. Matranga *et al.*, J. Phys. Chem. B **107**, 12930 (2003).
[72] K. A. Williams and P. C. Eklund, Chem. Phys. Lett. **320**, 352 (2000).
[73] M. R. Smith *et al.*, J. Phys. Chem. B **107**, 3752 (2003).
[74] Q. Wang, S. R. Challa, D. S. Sholl, and J. K. Johnson, Phys. Rev. Lett. **82**, 956 (1999).
[75] S. R. Challa, D. S. Sholl, and J. K. Johnson, J. Chem. Phys. **116**, 814 (2002).
[76] R. Q. Long and R. T. Yang, Ind. Eng. Chem. Res. **40**, 4288 (2001).
[77] O. Byl *et al.*, J. Am. Chem. Soc. **125**, 5889 (2003).
[78] J. W. Jiang and S. I. Sandler, Langmuir **20**, 10910 (2004).
[79] E. B. Mackie *et al.*, Langmuir **13**, 7197 (1997).
[80] E. B. Mackie, D. H. Galvan, and A. D. Migone, Adsorption **6**, 169 (2000).
[81] S. Talapatra, V. Krungleviciute, and A. D. Migone, Phys. Rev. Lett. **89**, 246106 (2002).
[82] J. Hilding *et al.*, Langmuir **17**, 7540 (2001).
[83] X. R. Zhang and W. C. Wang, Fluid Phase Equilib. **194**, 289 (2002).
[84] D. P. Cao *et al.*, J. Phys. Chem. B **107**, 13286 (2003).
[85] X. R. Zhang and W. C. Wang, Phys. Chem. Chem. Phys. **4**, 3048 (2002).
[86] S. Y. Bhide and S. Yashonath, J. Am. Chem. Soc. **125**, 7425 (2003).
[87] S. Supple and N. Quirke, Phys. Rev. Lett. **90**, 214501 (2003).
[88] J. P. Ryckaert and A. Bellemans, Faraday Discuss. Chem. Soc. **66**, 95 (1978).
[89] M. D. Macedonia and E. J. Maginn, Fluid Phase Equilib. **158–160**, 19 (1999).
[90] M. G. Martin and J. I. Siepmann, J. Phys. Chem. B **102**, 2569 (1998).
[91] M. G. Martin and J. I. Siepmann, J. Phys. Chem. B **103**, 4508 (1999).
[92] P. van der Ploeg and H. J. C. Berendsen, J. Chem. Phys. **76**, 3271 (1982).
[93] Y. Wang, K. Hill, and J. G. Harris, J. Chem. Phys. **100**, 3276 (1993).
[94] W. L. Jorgensen, J. D. Madura, and C. J. Swenson, J. Am. Chem. Soc. **106**, 813 (1984).
[95] F. Siperstein, A. L. Myers, and O. Talu, Mol. Phys. **100**, 2025 (2002).
[96] A. Thess *et al.*, Science **273**, 483 (1996).
[97] C. Journet *et al.*, Nature (London) **388**, 756 (1997).
[98] T. J. H. Vlugt and M. Schenk, J. Phys. Chem. B **106**, 12757 (2002).
[99] D. Frenkel and B. Smit, *Understanding Molecular Simulations: From Algorithms to Applications* (Academic, San Diego, 2002).
[100] K. Esselink, L. D. J. C. Loyens, and B. Smit, Phys. Rev. E **51**, 1560 (1995).
[101] B. Widom, J. Chem. Phys. **39**, 2802 (1963).
[102] D. Kofke, Mol. Simul. **7**, 285 (1991).
[103] J. W. Jiang and S. I. Sandler, Langmuir **19**, 5936 (2003).
[104] J. Talbot, AIChE J. **43**, 2471 (1997).
[105] M. Heuchel, Langmuir **13**, 1150 (1997).
[106] J. R. Arnold, J. Am. Chem. Soc. **71**, 104 (1949).
[107] T. Dumitrica, C. M. Landis, and B. I. Yakobson, Chem. Phys. Lett. **360**, 182 (2002).
[108] M. K. Kostov, H. Cheng, A. C. Cooper, and G. P. Pez, Phys. Rev. Lett. **89**, 146105 (2002).
[109] L. A. Clark, M. Sierka, and J. Sauer, J. Am. Chem. Soc. **125**, 2136 (2003).
[110] J. B. Klauda *et al.*, J. Phys. Chem. A **108**, 107 (2004).
[111] J. B. Klauda, J. W. Jiang, and S. I. Sandler, J. Phys. Chem. B **108**, 9842 (2004).
[112] J. W. Jiang, J. B. Klauda, and S. I. Sandler, J. Phys. Chem. B **108**, 9852 (2004).
[113] J. W. Jiang, J. B. Klauda, and S. I. Sandler, J. Phys. Chem. B **109**, 4731 (2005).